Observational evidence of European summer weather patterns predictable from spring

Observational evidence of European summer weather patterns predictable from spring

Albert Ossó[a,1], Rowan Sutton[a], Len Shaffrey[a], and Buwen Dong[a]

[a]Department of Meteorology, National Centre for Atmospheric Science, University of Reading, Reading RG6 6BB, United Kingdom

Edited by Ben Kirtman, University of Miami, Miami, FL and accepted by Editorial Board Member Robert E. Dickinson November 10, 2017 (received for review July 24, 2017)

Forecasts of summer weather patterns months in advance would be of great value for a wide range of applications. However, seasonal dynamical model forecasts for European summers have very little skill, particularly for rainfall. It has not been clear whether this low skill reflects inherent unpredictability of summer weather or, alternatively, is a consequence of weaknesses in current forecast systems. Here we analyze atmosphere and ocean observations and identify evidence that a specific pattern of summertime atmospheric circulation—the summer East Atlantic (SEA) pattern—is predictable from the previous spring. An index of North Atlantic sea-surface temperatures in March–April can predict the SEA pattern in July–August with a cross-validated correlation skill above 0.6. Our analyses show that the sea-surface temperatures influence atmospheric circulation and the position of the jet stream over the North Atlantic. The SEA pattern has a particularly strong influence on rainfall in the British Isles, which we find can also be predicted months ahead with a significant skill of 0.56. Our results have immediate application to empirical forecasts of summer rainfall for the United Kingdom, Ireland, and northern France and also suggest that current dynamical model forecast systems have large potential for improvement.

climate variability | seasonal forecast | sea–air interactions | predictability

In 1964, Bjerknes (1) placed the foundations to our current understanding of ocean–atmosphere interactions. Since then, there has been great progress in understanding how these interactions shape patterns of weather and climate around the world, and how they can be exploited to deliver predictions for lead times ranging from days to centuries. Seasonal forecasting targets lead times of 1–6 months. Developments in seasonal forecasting have focused especially on the tropical El Niño Southern Oscillation (ENSO) phenomenon and its impacts. Seasonal forecasts have highest skill in the tropics (2), but there is also some skill in the extratropics especially during winter, partly associated with the remote impacts of ENSO (3). By contrast, seasonal forecasts for the extratropics in summer have lower skill (4, 5). In particular, current dynamical models show very little skill for European summers (6, 7). This low skill might reflect inherent unpredictability, but it is also possible that it reflects our still incomplete understanding of ocean–atmosphere interactions and the imperfect representation of these interactions in current forecast systems. In that case, there may be potential for much more skillful, and useful, summer forecasts.

Previous work has suggested a link between European summer climate and preceding North Atlantic sea-surface temperature (SST) (8–11). In particular, a recent study (12) used maximum covariance analysis (MCA) to show that a summertime (June–August) North Atlantic sea-level pressure (SLP) anomaly covaries with a preceding spring (March–May) (SST) pattern. In this study we investigate in greater depth the relationship between spring SST and summertime atmospheric circulation in the North Atlantic, and explore the potential to exploit this relationship to generate skillful forecasts of European summer weather. We use bimonthly averaged observations of ocean and atmosphere variables from the ERA Interim reanalysis dataset for the period 1979–2015 and other data sets (*Methods*).

Following Gastineau and Frankignoul (12), we applied MCA analysis to the ERA Interim data. Fig. S1 illustrates how a pattern of SST anomalies in March–April (MA) covaries significantly with an SLP anomaly in the subsequent July–August (JA). The SLP anomaly is located west of the United Kingdom and we describe this as the summer East Atlantic (SEA) pattern.

To obtain further insight into the precursor SST signals we perform a lagged linear regression analysis (Fig. 1 and Fig. S2) between bimonthly precursor SST and SLP anomalies and an SLP index for the JA SEA pattern (*Methods*). This analysis shows that positive (anticyclonic) anomalies in the JA SEA pattern are preceded by a dipolar pattern of SST anomalies, with warm anomalies east of Newfoundland and cool anomalies west of the Iberian Peninsula. The SST dipole pattern is present in late winter and becomes stronger (in terms of both amplitude and correlations) in spring (MA and AM). The SST anomalies are weaker in late spring and early summer (MJ and JJ). The simultaneous anomalies (JA) are the strongest, although the SST pattern has evolved with the largest warm anomalies now located in the northeast Atlantic on the western side of the SEA pattern. There are also precursor SLP anomalies, in particular a dipolar pattern in late winter and early spring (FM and MA). In AM the anticyclonic component over the northwest Atlantic becomes more dominant, whereas in MJ circulation anomalies are very weak.

We further investigate the ocean–atmospheric interactions implied in Fig. 1 by calculating the bimonthly upper ocean temperature tendencies due to anomalous turbulent surface fluxes and

Significance

Forecasts of summer weather patterns months in advance would be of great value for a wide range of applications, from tourism to agriculture, water resource management, energy production, construction, and retail. However, dynamical model seasonal forecasts for European summers have very little skill. Here, we analyze atmosphere and ocean observations and identify evidence that a specific pattern of summertime atmospheric circulation over Western Europe is predictable from the previous spring North Atlantic sea-surface temperatures, and identify the mechanism involved. The atmospheric pattern has a particularly strong influence on rainfall in the British Isles and in the north coast of France, which we find can also be predicted months ahead with significant skill.

Author contributions: A.O., R.S., and L.S. designed research; A.O., R.S., L.S., and B.D. performed research; B.D. contributed new analytic tools; A.O. analyzed data; and A.O. and R.S. wrote the paper.

The authors declare no conflict of interest.

This article is a PNAS Direct Submission. B.K. is a guest editor invited by the Editorial Board.

[1]To whom correspondence should be addressed. Email: a.osso@reading.ac.uk.

This article contains supporting information online at www.pnas.org/lookup/suppl/doi:10.1073/pnas.1713146114/-/DCSupplemental.

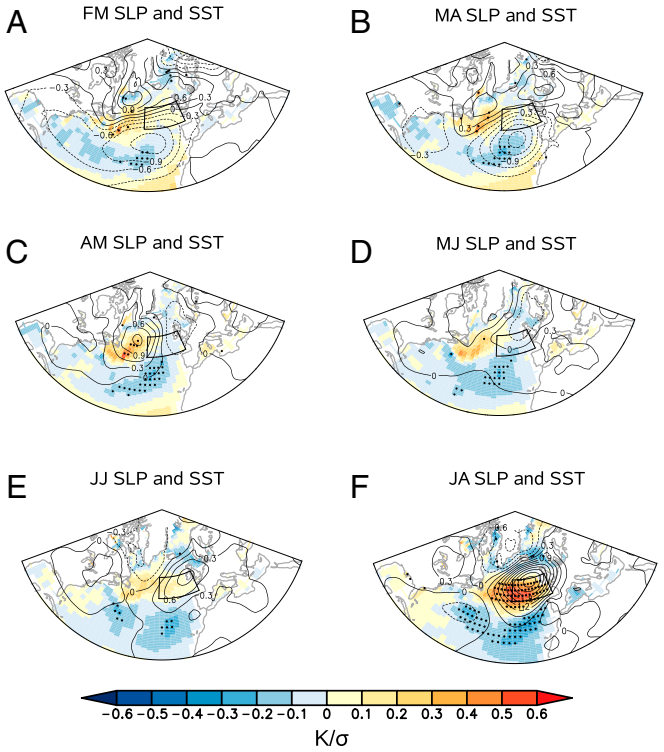

Fig. 1. Linear regressions of bimonthly precursor SST and SLP anomalies against the SLP index of the JA SEA pattern. (*A*–*F*) Regression maps of the indicated bimonthly SST (shading) and SLP (contours) anomalies against the SLP index for the JA SEA pattern (*Methods*). The SLP index is normalized; thus, the SST and SLP anomalies shown correspond to an SD of the SLP index time series. Contour interval is 0.3 hPa σ^{-1}. Stippling indicates SST regression coefficients statistically significant at the 95% confidence level (*Methods*). The black box indicates the region used to calculate the SLP index.

Ekman advection (Fig. S3). These results suggest the warm anomaly east of Newfoundland is generated by anomalous turbulent heat flux and Ekman advection associated with weaker westerly winds during late winter and early spring (FM and MA), whereas the cool anomaly is forced primarily by anomalous turbulent heat lost during MA. There is a small additional contribution to the SST tendency in FM and MA, particularly in the region of the cool anomaly, from anomalous Ekman upwelling raising or lowering the thermocline. In MJ, turbulent surface flux anomalies act to damp the warm anomaly, consistent with the weak circulation anomalies and the falling magnitude of the SST anomaly at this time. In JA, increased surface short-wave radiation and reduced upward turbulent surface flux anomalies both act to warm the SST in the region of the largest warm anomaly with a secondary contribution from Ekman advection.

From these results we hypothesize that spring SST anomalies, generated largely by atmospheric forcing, persist into summer and then influence atmospheric circulation. We test this idea further by regressing on an index for the spring (MA) SST dipole (*Methods*, Fig. 2, and Fig. S4). Positive values of this index are associated with warm anomalies east of Newfoundland and cool anomalies west of Iberia. Note that since the typical persistence time of the atmosphere is about 1 month, a significant regression coefficient between the SST index and SLP, when the former is leading by more than 1 month, suggests the ocean may be forcing the atmosphere.

The evolution of the SST dipole in Fig. 2 is consistent with Fig. 1: The dipolar pattern intensifies in AM, weakens a little in MJ, and then intensifies further in JA with the warm SST anomalies moving eastward. The evolution of the SLP anomalies is also consistent with Fig. 1, but the strengthening of the SLP anomalies in JA, both in amplitude and correlation (Fig. S4), is particularly notable. Whereas Fig. 1*F* shows simultaneous regressions, Fig. 2*D* shows regressions on an SST predictor 4 months earlier. Fig. S4 shows that the SLP correlation on the MA SST index increases from an insignificant level (~0.2) in MJ, to a highly significant level (>0.6) in JA. In Fig. 1*F*, it is not possible to distinguish the ocean's influence on the atmosphere from the atmosphere's influence on the ocean, but Fig. 2 and Fig. S4 clearly suggest that the SST anomalies force a significant atmospheric response in JA. Analysis of geopotential height anomalies at different pressure levels shows that the atmospheric response has an equivalent barotropic vertical structure (Fig. S5).

Interestingly, our results suggest a possible positive feedback in JA between atmospheric circulation and SSTs. Fig. 2 and Fig. S4 suggest that positive values of the SST dipole index force anticyclonic SEA pattern anomalies, meanwhile Fig. S3 suggests that anticyclonic SEA pattern anomalies force a warming of SSTs, which acts to increase the amplitude of the SST dipole, so potentially generating a positive feedback. Such a feedback could help to explain the increase in the amplitude and spatial scale of the positive SST anomalies between MJ and JA seen in Fig. 2 *C* and *D* and the high SLP correlations seen in JA of Fig. S4*D*.

These results raise the question of what is the physical mechanism by which the SST dipole forces the SEA pattern, and why the atmosphere responds to the SST dipole primarily in JA. We suggest that the SEA pattern is the surface fingerprint of a poleward displacement of the North Atlantic jet stream, forced by changes in baroclinicity and in the transient eddy activity (momentum convergence) associated with the SST dipole. Regression of JA 850-hPa zonal wind anomalies on the MA SST index are consistent with the jet speed responding directly to anomalies in the meridional SST gradient, measured by the SST dipole index (Fig. 3). When the SST index is positive (weakening the meridional SST gradient in the subtropics and enhancing it in the subpolar North Atlantic), this response is associated with a poleward displacement of the jet, manifest at the surface as an anticyclonic (high SLP) anomaly in the SEA pattern. Analysis of the Eady growth rate (13) (Fig. S6) (a measure of baroclinicity) suggests that the jet displacement is associated with changes in the meridional gradient of SST, with a weakening of the jet downstream of the region where the SST gradient is reduced and an enhancement of it to the north where the SST gradient is increased. Changes in static stability play only a secondary role. The equivalent barotropic nature of the circulation anomalies (Fig. S5) is consistent with an important role for transient eddy activity in establishing the atmospheric response.

The timing of the atmospheric response is likely to be a consequence of the seasonal evolution of the jet. The jet maximum is generally located close to the regions of largest baroclinicity (14). During wintertime, the jet maximum is situated over the American East Coast in the region of the large temperature gradients between the land and the ocean. However, the jet moves northward and eastward during spring and summer as the descending branch of the Hadley Circulation moves poleward and the North American continent warms up (15, 16). We hypothesize that during JA this seasonal evolution places the jet in a location where it has enhanced sensitivity to the variations in baroclinicity associated with the SST dipole index. The fact that the correlations between SLP and the MA SST index (shown in Fig. S4) initially decline (from MA to MJ) and then increase very substantially in JA further supports the above hypothesis.

The SEA pattern affects summertime weather in Western Europe and our results suggest the potential for useful predictions from the preceding spring. We use a multilinear regression model to illustrate the potential skill of spring SST to predict the summer time SLP and rainfall over Europe. The model consists of two terms, the first modeling the interannual variations and

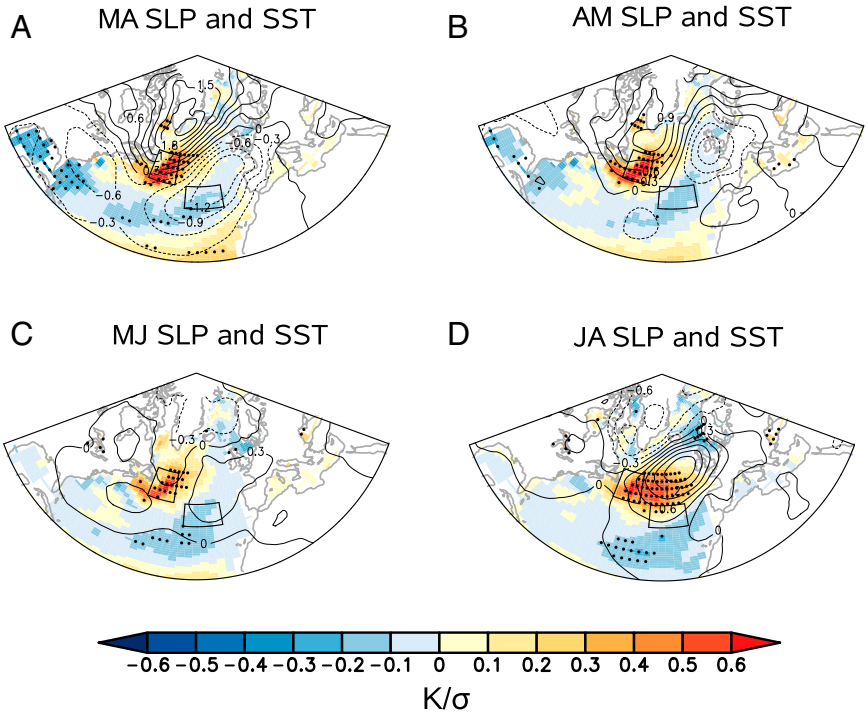

Fig. 2. (*A–D*) Linear regression maps of the indicated bimonthly SST (shading) and SLP (contours) against the precursor MA SST index. The SST index is normalized; thus, the SST and SLP anomalies shown correspond to an SD of the SST index time series. Contour interval is 0.3 hPa σ^{-1}. Stippling indicates SST regression coefficients statistically significant at the 95% confidence level (*Methods*). The black boxes indicate the regions used for the SST index, which is calculated as the SST average of the northern box minus the SST average of the southern box.

the second modeling the low-frequency variations and trends (*Methods*). Fig. 4 shows that JA SLP variations in the SEA region can be predicted from the preceding MA SST index with a significant cross-validated correlation skill of 0.67 ($P < 0.01$). There is also a relationship to rainfall, especially in the United Kingdom, Ireland, and northern France; rainfall in this region can be predicted with a significant correlation skill of 0.56 ($P < 0.01$) with less summer rainfall associated with positive MA SST index.

One important issue is the relation between this study and previous work showing the existence of a relationship on multidecadal timescales between North Atlantic SSTs (associated with a positive phase of the Atlantic Multidecadal Oscillation, AMO) and the atmospheric circulation (10, 11). The summertime atmospheric response to the AMO appears to be baroclinic, with a structure characteristic of a linear stationary wave response (10). By contrast, the evidence of our study is that interannual variability is associated with a different, transient eddy-dominated, mechanism and an equivalent barotropic response. We have confirmed that our results are dominated by interannual timescales by examining sensitivity to prefiltering the data (*Methods*). The reason why different responses are important on different timescales is an important topic for future research, although it should be noted that the SST patterns associated with interannual and multidecadal variability differ.

Our results provide an immediate basis for empirical forecasts of important aspects of European summer weather. Even more importantly, they suggest that the potential for improving dynamical model seasonal forecasts of European summers is very considerable. These improvements in seasonal forecast systems might include improving the representation of air–sea interactions, increasing model resolution, and reducing model biases, especially biases affecting the position and intensity of the jet stream. Such forecasts could be of very high value for applications ranging from tourism to agriculture, construction, and retail. Realizing this potential will require further advances in numerical modeling and forecast systems, and in fundamental understanding of ocean–atmosphere interactions.

Methods

Observational Data. The mean SLP, SST, zonal and meridional wind, surface air temperature, surface radiation, and surface turbulent fluxes are based on 2.5° × 2.5° gridded monthly averaged output for the period 1979–2015 from the European Center for Medium-Range Weather Forecast Interim reanalysis dataset (17). European daily precipitation is retrieved from the European Climate Assessment & Dataset (E-OBS) dataset at a 0.25° × 0.25° spatial resolution (18). The regions where sea-ice coverage exceeds 1% are excluded from the SST field.

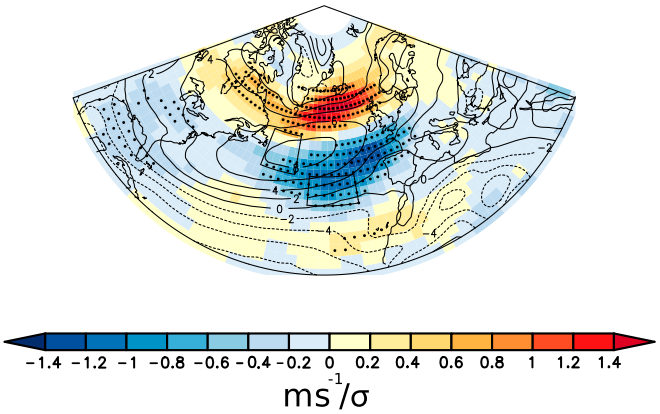

Fig. 3. Linear regression map of JA zonal wind anomalies at 850 hPa (U850) against the precursor MA SST index (shading). The SST index is normalized; thus, the zonal wind anomalies shown correspond to an SD of the SST index time series. Contours show the JA U850 climatology. Contour interval is 2 ms^{-1}. Stippling indicates U850 regression coefficients statistically significant at the 95% confidence level (*Methods*).

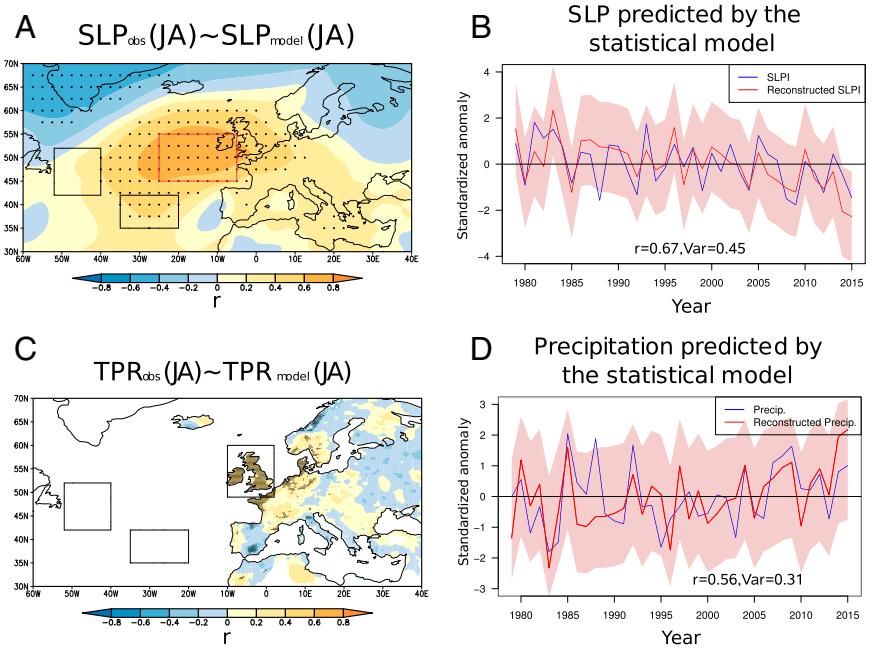

Fig. 4. (*A*) Cross-validated correlation of JA mean SLP anomalies predicted by the statistical model against observed raw JA mean SLP anomalies. (*B*) Normalized time series of observed raw JA mean SLP anomalies (solid blue) and JA mean SLP anomalies predicted by the statistical model applying a leave-one-out cross-validation method (solid red) with the 95% confidence predictive interval (pink shading) (*Methods*). Both time series are spatially averaged over the east Atlantic box displayed in *A*. (*C*) Cross-validated correlation of JA mean E-OBS precipitation anomalies predicted by the statistical model against observed raw JA mean E-OBS precipitation anomalies. (*D*) As in *C* but for E-OBS precipitation time series. Note that the sign of the SST index has been reversed to facilitate comparison. The correlation coefficient (*r*) and the percentage of variance (Var) explained by the statistical model are indicated in *B* and *D*. Both correlation coefficients are statistically significant above the 99% confidence level (*Methods*).

Analysis. Bimonthly averages are calculated from monthly mean data and from daily mean for the E-OBS data. All of the analysis is carried out with bimonthly averaged anomalies calculated by subtracting the corresponding bimonthly climatology. The use of 2-month averages is a compromise which provides insight into the seasonal evolution of anomalies while maintaining higher signal-to-noise than is associated with a monthly analysis. However, using monthly instead of bimonthly average data does not change the results and conclusions of this analysis. All data are linearly detrended to focus on interannual variability (see the subsection *Results Sensitivity to Detrending and High Pass Filtering*).

MCA (Fig. S1) is used to identify the covariability patterns between bimonthly averaged JA SLP and leading bimonthly SST anomalies in MA over the North Atlantic region (20°N–70°N; 90°W–30°E). As the intrinsic atmosphere persistence is less than 1 month, when the SST leads the atmosphere by more than 1 month a significant covariance pattern may indicate ocean forcing of the atmosphere (12, 19). MCA consists of a singular-value decomposition of the joint area-weighted SLP and SST covariance matrix and provides a pair of spatial patterns with an associated time series for each covariability mode. The statistical significance of each mode is tested as in Gastineau and Frankignoul (12) by Monte Carlo methods that account for the serial autocorrelation of the SLP time series. The MCA results are presented in terms of regressions between the normalized MCA time series and the SLP and SST anomalies at every grid point. The variance fraction of the SLP explained by the SST is given by the squared covariance of the correlation coefficient between the MCA time series.

The SLP index is calculated by averaging the JA SLP anomalies over the SEA region (45°N–55°N; 25°W–5°W) indicated with a black box in Fig. 1. Note that the results are not sensitive to small variations on the domain used to define the SLP index. The SLP index is standardized so that it has mean of zero and SD of 1.

The SST index is calculated by averaging the MA SST over the north western box in Fig. 2*A* (42°N–52°N; 52°W–40°W) minus the MA SST averaged over the south eastern box (35°N–42°N; 35° W–20°W). The results are not sensitive to small variations on the domain used to define the SST index. The SST index is standardized as for the SLP index.

Linear regression and correlation analyses are performed to identify the lead–lag relationship between a pair of variables. The statistical significance of the linear regressions and correlations is estimated using a two-tailed Student-*t* test with adjusted degrees of freedom to account for the autocorrelation of the time series following the methodology outlined in Santer et al. (20).

Statistical Model. The statistical prediction model is based on multilinear regression where the predictand is the JA SLP or rainfall anomalies. To take into account that both terms exhibit interannual and low-frequency variability (Fig. S7), the model is composed of two terms: the first term uses the raw (nondetrended) MA SST anomalies as a predictor to model interannual variations and the second term uses a linear trend to model low-frequency variations. The model can be written as follows:

$$SLP(JA) = A * SSTI(MA) + B * t,$$

where *A* and *B* are the linear regression coefficients adjusted by least-squares and *t* is a linear trend normalized to have variance of 1. The statistical prediction model is cross-validated with a 1-y-out method (21).

Results Sensitivity to Detrending and High-Pass Filtering. North Atlantic SST and atmospheric variability are modulated by low-frequency modes and global warming. The SLP over the SEA region and the SST index exhibit opposite trends for the period 1979–2015. To assess whether the opposite trends are not due to the relatively short length of the ERA Interim data set, we analyzed the HadISST (22) and HadSLP2r (23) data products for the period 1870–2015. Fig. S7 shows that in addition to the year-to year variability which is the focus of attention in this study the two time series exhibit an out of phase low-frequency component, consistent with the expectation that other processes are important on multidecadal timescales. As shown in Fig. S7, this low-frequency component can be modeled by a third-order polynomial. However, over the period of interest (1979–2016) the low-frequency component can be modeled more simply as a linear trend.

Detrending the data does not change the regression or correlation spatial patterns but it affects the magnitude of the regression and correlation coefficients, and the skill of the statistical model. If the linear trend term is excluded from the statistical model the correlation skill for the SLP index is reduced to 0.45 ($P < 0.05$) when using raw data, or 0.61 ($P < 0.01$) if the data are detrended first. The correlation skill for the rainfall averaged over the

box shown in Fig. 4 is reduced to 0.41 ($P < 0.05$) when using raw data, or 0.50 ($P < 0.05$) if the data are detrended first.

We also investigated the sensitivity of our results to high-pass filtering by removing a 5-y running mean and repeating the analyses. The effect on our results was very small, confirming that they are dominated by interannual rather than lower-frequency variability.

Mixed-Layer Ocean Temperature Tendency. The monthly mixed-layer ocean temperature tendency due to changes in surface radiation, surface turbulent heat flux, and Ekman transport is calculated using monthly mean SST, wind stress, surface short- and long-wave radiation flux, and surface sensible and latent heat flux of the ERA-Interim reanalysis.

The temperature tendency associated with Ekman transport is calculated at each grid point as the product between the zonal and meridional Ekman velocity and the zonal and meridional monthly mean SST gradient, respectively. The Ekman velocity is calculated from the wind stress using an Ekman layer depth of 40 m.

The temperature tendency associated with radiative and turbulent heat flux is calculated at each grid point as the radiative or turbulent heat flux divided by the product of the seawater density (1,029 kg m^{-3}), the heat capacity (4,182.0 J $kg^{-1}{\cdot}K^{-1}$), and the mixed-layer depth (meters). We use a seasonally and spatially varying mixed-layer depth climatology from the French Research Institute for Exploration of the Sea based on a fixed threshold criterion of 0.2° C (24).

The ocean mixed-layer temperature tendency calculation is subject to a number of uncertainties: (*i*) All of the data but especially the surface fluxes (thermal and radiation) are subject to uncertainties (17); (*ii*) The seasonal and spatial evolution of the mixed-layer depth is as well subject to uncertainties and the use of the 0.2 °C criterion to define the mixed-layer depth may not always hold in the real world; and (*iii*) The impact of some secondary processes, for example the geostrophic currents, are not included in the calculation.

ACKNOWLEDGMENTS. This work was supported by the SummerTIME project funded through the Natural Environment Research Council (NERC) Drivers of Variability in Atmospheric Circulation program and the NERC IMPETUS project. A.O., L.S., B.D., and R.S. are supported by the UK National Centre for Atmospheric Science, including the North Atlantic Climate System Integrated Study project.

1. Bjerknes J (1964) Atlantic air-sea interaction. *Adv Geophys* 10:1–82.
2. Kirtman BP, Piran A (2009) The state of the art of seasonal prediction: Outcomes and recommendations from the First World Climate research program Workshop on Seasonal prediction. *Bull Am Meteorol Soc* 90:455–458.
3. Scaife AA, et al. (2014) Skillful long-range prediction of European and North American winters. *Geophys Res Lett* 41:2514–2519.
4. Arribas A, et al. (2011) The GloSea4 ensemble prediction system for seasonal forecasting. *Mon Weather Rev* 139:1891–1910.
5. Qian B, Saunders M (2003) Summer U.K. temperature and its links to preceding Eurasian snow cover, North Atlantic SST and the NAO. *J Clim* 16:4108–4120.
6. Prodhomme C, Doblas-Reyes F, Bellprat O, Dutra E (2016) Impact of land-surface initialization on sub-seasonal to seasonal forecasts over Europe. *Clim Dyn* 47:919–935.
7. Ardilouze C, et al. (2017) Multi-model assessment of the impact of soil moisture initialization on mid-latitude summer predictability. *Clim Dyn* 49:3959–3974.
8. Colman A (1997) Prediction of summer central England temperature from preceding North Atlantic winter sea surface temperature. *Int J Climatol* 17:1285–1300.
9. Colman A, Davey MK (1999) Prediction of summer temperature, rainfall and pressure in Europe from preceding winter North Atlantic Ocean temperature. *Int J Climatol* 19: 513–536.
10. Ghosh R, Müller WA, Baehr J, Bader J (2017) Impact of observed North Atlantic multidecadal variations to European summer climate: A linear baroclinic response to surface heating. *Clim Dyn* 48:3547–3563.
11. Sutton RT, Hodson DL (2005) Atlantic Ocean forcing of North American and European summer climate. *Science* 309:115–118.
12. Gastineau G, Frankignoul C (2015) Influence of the North Atlantic SST variability on the atmospheric circulation during the twentieth century. *J Clim* 28:1396–1416.
13. Eady ET (1949) Long waves and cyclone waves. *Tellus* 1:33–52.
14. Woollings T, Hannachi A, Hoskins B (2010) Variability of the North Atlantic eddy-driven jet stream. *Q J R Meteorol Soc* 136:856–868.
15. Hoskins BJ, Valdes PJ (1990) On the existence of storm-tracks. *J Atmos Sci* 47: 1854–1864.
16. Wallace JM, Zhang Y, Lau KH (1993) Structure and seasonality of interannual and interdecadal variability of the geopotential height and temperature fields in the Northern Hemisphere troposphere. *J Clim* 6:2063–2082.
17. Dee DP, et al. (2011) The ERA-interim reanalysis: Configuration and performance of the data assimilation system. *Q J R Meteorol Soc* 137:553–597.
18. Haylock MR, et al. (2008) A European daily high-resolution gridded data set of surface temperature and precipitation for 1950–2006. *J Geophys Res Atmos* 113:D20119.
19. Czaja A, Frankignoul C (2002) Observed impact of Atlantic SST anomalies on the North Atlantic oscillation. *J Clim* 15:606–623.
20. Santer BD, et al. (2008) Consistency of modelled and observed temperature trends in the tropical troposphere. *Int J Climatol* 28:1703–1722.
21. Coelho CAS, Pezzulli S, Balmaseda M, Doblas-Reyes FJ, Stephenson DB (2004) Forecast calibration and combination: A simple Bayesian approach for ENSO. *J Clim* 17: 1504–1516.
22. Rayner NA, et al. (2003) Global analyses of sea surface temperature, sea ice, and night marine air temperature since the late nineteenth century. *J Geophys Res Atmos* 108: 4407.
23. Allan RJ, Ansell TJ (2006) A new globally complete monthly historical gridded mean sea level pressure dataset (HadSLP2): 1850-2004. *J Clim* 19:5816–5842.
24. De Boyer Montégut C, Madec G, Fischer AS, Lazar A, Ludicone D (2004) Mixed layer depth over the global ocean: An examination of profile data and a profile-based climatology. *J Geophys Res Oceans* 109:C12003.